COMMUNICATION

Two Heads are Better than One: Improving Magnetic Relaxation in the Dysprosium Metallocene $DyCp^*_2BPh_4$ Upon Dimerization by Use of an Exceptionally Weakly-Coordinating Anion

Received 00th Month 20xx,
Accepted 00th Month 20xx

DOI: 10.1039/x0xx00000x

Dylan Errulat,[a] Bulat Gabidullin,[b] Akseli Mansikkamaki[c] and Muralee Murugesu[a]*

Partial metathesis between two weakly-coordinating anions in the archetypical dysprosium metallocene $DyCp^*_2BPh_4$ results in the first example of $[BPh_4]^-$ as a bridging ligand in 4f metals, with a unique $\eta_2, \eta_2 : \eta_2, \eta_2$-bridge. Magnetic susceptibility and relaxation dynamics studies along with *ab initio* calculations reveal improved slow relaxation of the magnetization in $[Dy_2Cp^*_4(\mu\text{-}BPh_4)][Al(OC(CF_3)_3)_4]$ over its mononuclear congener, resulting in an energy barrier of 298 K / 340 cm^{-1} and waist-restriced hysteresis up to 6.5 K.

The complex $LnCp^*_2BPh_4$ (Ln = Lanthanide, Cp* = 1,2,3,4,5-Pentamethylcyclopentadiene) is archetypal in the field of lanthanide chemistry as a means of introducing diverse properties to Ln-based organometallic frameworks. The weak coordination of the tetraphenylborate anion lends itself well to facile ligand exchange, allowing us to impart various structural and electronic changes to afford new and interesting properties, such as redox behaviour, small molecule activation, and magnetic properties to these systems.[1–4] This complex is largely responsible for many of the advances in Ln-based Single-Molecule Magnets (SMMs), paving the way for the high performing single-ion magnets,[5–7] and bridged multinuclear SMMs we see today.[8–12] Dinuclear SMMs are of particular interest as even weak couplings between metal centres is known to reduce the effects of ground state quantum tunnelling of the magnetization (QTM), a phenomenon which largely plagues the performance of 4f-based SMMs.[13] Such systems have been synthetically possible *via* exchange with stronger donating ligands to replace the weak agostic interactions of the $[BPh_4]^-$. Unfortunately, in the case of magnetic properties of Dy-based systems the pseudo-linear coordination of the Cp-type ligands are responsible for the uniaxial magnetic anisotropy,[14] and thus this ligand exchange may in fact be deleterious to the height of the energy barrier by perturbing the magnetic axis towards the equatorial plane in the higher excited states.[15–18] With this in mind, we sought to employ a weaker bridging motif to create multinuclear complexes while maintaining strong uniaxial magnetic anisotropy. We report the successful application of this concept to the well-known $DyCp^*_2BPh_4$ itself by use of an extremely weakly-coordinating perfluorinated alkoxyaluminate anion, leading to the isolation of the dinuclear complex $[Cp^*_4Dy_2(\mu\text{-}BPh_4)][Al(OC(CF_3)_3)_4]$ (**1**). A first in *4f*-chemistry, this is one of the few example in which $[BPh_4]^-$ is shown to act as a bridging ligand,[19–21] doing so through a never-before seen $\eta_2,\eta_2:\eta_2,\eta_2$-bridge. The weakly coordinating anion (WCA) $[Al(OC(CF_3)_3)_4]^-$ has been utilized to stabilize highly reactive main group and transition metal species.[22–24] Yet, to date remains relatively underrepresented in *4f*-chemistry.[25,26] This anion is utilized herein to yield **1** as a cationic dimer that would likely not be accessible with the more strongly coordinating borate-based WCAs which are most common. Surprisingly, magnetic susceptibility measurements reveal impressive slow relaxation dynamics, exhibiting improved magnetic properties compared to the model mononuclear counterpart.

$[Dy_2Cp^*_4(\mu\text{-}BPh_4)][Al(OC(CF_3)_3)_4]$ (**1**) was obtained from the reaction between $Li[Al(OC(CF_3)_3)_4]$ and 2 equivalents of $DyCp^*_2BPh_4$ in toluene. To overcome the poor solubility of the two starting materials, sonication at elevated temperatures was employed to produce **1** in sufficient yield (see ESI). Complex **1** crystalizes with three molecules of toluene in the *P* $2_1/c$ space group as a cationic dinuclear complex in which two bent Dy^{III} metallocene units are bridged by a $[BPh_4]^-$ anion through agostic interactions to all four phenyl rings, orienting the metallocene units non-parallel to one another (Fig. 1). The overall charge of the complex is balanced by $[Al(OC(CF_3)_3)_4]^-$ as a charge-separated pair on account of the significantly reduced charge-surface of $[Al(OC(CF_3)_3)_4]^-$ compared to $[BPh_4]^-$.[27] While $[BPh_4]^-$ and other arene-type ligands have been well documented to coordinate to electron-deficient metal centers,[28,29] there exists

[a] Department of Chemistry and Biomolecular Sciences, University of Ottawa, Ottawa, ON K1N 6N5, Canada.
[b] Canadian Light Source Inc. Saskatoon, SK S7N 2V3, Canada.
[c] NMR Research Unit, University of Oulu, P. O. Box 3000, 90014 Oulu, Finland.
† Corresponding Author: M. Murugesu (E-mail: m.murugesu@uottawa.ca)
Electronic Supplementary Information (ESI) available: DOI: 10.1039/x0xx00000x

very few examples of bridging $[BPh_4]^-$ in the literature, and to date have been limited to a few closely related Rh^{III} ethylene complexes and metal-metal bound Ni^{I} phosphines.[19–21]

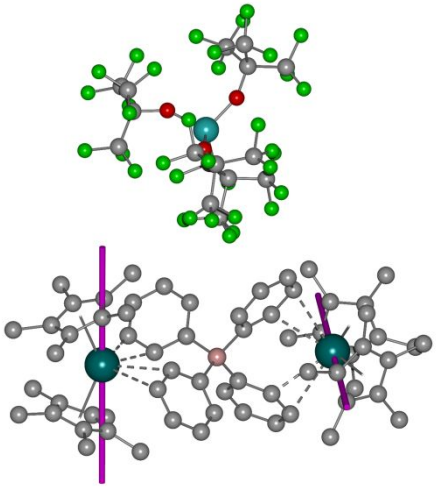

Fig. 1 Molecular structure of $[Cp^*_4Dy_2(\mu\text{-}BPh_4)][Al(OC(CF_3)_3)_4]$ (**1**). Orientation of the principal magnetic axes of the ground Kramers doublet is depicted as a magenta line. Hydrogen atoms and solvent molecules are omitted for clarity. Colour code: Dy: cyan; Al: teal; B: beige; C: grey; O: red; F: green.

The metal centres are separated by an intramolecular Dy···Dy distance of 9.07 Å, while the closest Dy···Dy intermolecular distance is slightly shorter at 9.04 Å. Unsurprisingly, an overlay of the molecular structures of the parent $DyCp^*_2BPh_4$ and $[Dy_2Cp^*_4(\mu\text{-}BPh_4)]^+$ reveal close similarities (Fig. S1), however, several structural differences are worth noting. Particularly, dimerization leads to rotation of the phenyl rings of $[BPh_4]^-$ by 65° and 70° to accommodate coordination of the sterically encumbered metallocene. It is noteworthy that complex **1** is non-centrosymmetric with Dy2 having markedly reduced bond lengths to the phenyl rings than the parent complex by an average of 0.261 Å, while the Dy1 distance to the $[BPh_4]^-$ remains nearly unchanged when compared to the monometallic complex. Ultimately, this orientation favours greater $Cp^*_{centroid}\cdots Dy\cdots Cp^*_{centroid}$ angles in the dinuclear complex of 135.4° and 134.7°. While the monomer, containing two unique molecules in the unit cell, has marginally smaller angles of 133.6° and 134.0°.

Direct current susceptibility measurements performed on **1** reveal a room temperature molar magnetic susceptibility (χT) of 27.93 $cm^3\ K\ mol^{-1}$ under an applied static field of 1000 Oe is obtained (Fig. S4), which is consistent with the free-ion value of 28.34 $cm^3\ K\ mol^{-1}$ for two non-interacting Dy^{III} ions ($^6H_{15/2}$, S = 5/2, L = 5, g = 4/3). Upon cooling, the χT product decreases gradually until a rapid decrease can be observed below 25 K. The role of exchange and/or dipolar interactions in this downturn was examined by *ab initio* calculations using the point-dipolar approximation projected onto the ground Kramers doublets (KDs) at the Dy sites. The Ising-type dipolar coupling is 0.0014 cm^{-1}. Considering the long superexchange pathway, other exchange mechanisms were deemed to be negligible compared to the dipolar coupling. Taking into account the magnitude of the coupling interaction, the drop in the χT value at low temperature is most likely attributable to the depopulation of excited doublets in the ground manifold and/or magnetic blocking as a result of significant magnetic anisotropy.[30] The magnetization was probed up to 7 T, reaching saturation at a value of 8.52 μ_B at 1.8 K (Fig. S3). This value is smaller than what is expected based on the free ion (≈ 10 μ_B per Dy^{III}), but remains consistent with the degeneracy of the ground term ($^6H_{15/2}$) being lifted *via* the highly axial crystal field (< 6 μ_B per Dy^{III}).

The magnetic relaxation dynamics of **1** were investigated with the use of alternating current (AC) magnetic measurements (H_{ac} = 3.78 Oe and H_{dc} = 0 Oe). The in-phase ($\chi'(\nu)$; Fig. S5) and out-of-phase ($\chi''(\nu)$; Fig. 2) susceptibilities display distinct frequency-dependent behaviour within the studied temperature range of 2 – 55 K. In order to quantify the effects of the multiple relaxation pathways, temperature-dependent relaxation times (τ) were extracted by fitting the individual components of the $\chi'(\nu)$ and $\chi''(\nu)$ susceptibilities to the generalized Debye model (Table S2, S4).[31] By plotting the ln(τ) *vs.* T^{-1} obtained from the $\chi''(\nu)$, a strong linear dependence of ln(τ) at high temperatures is observed (Fig. 3), indicating relaxation *via* thermally activated processes resulting from relaxation through higher excited states. Upon decreasing temperature, ln(τ) *vs.* T^{-1} begins to deviate from linearity and displays a power relationship with temperature, indicative of Raman relaxation. At low temperatures, through-barrier mechanisms become increasingly operative and begin to define the rate of magnetic relaxation. Ground state QTM dominates the low-temperature behaviour below *ca.* 10 K resulting in a relative plateau of the relaxation times. The low-temperature region is also characterized by relatively large α parameters (≈ 0.35), likely as a result of the combined contributions of the two metal centres which reside in similar coordination environments leading to an unusually broad distribution of the relaxation times. Thus, in the absence of an applied static field, the zero-field magnetic susceptibility exhibits three distinct relaxation regimes which can be modelled by the sum of the thermally activated Orbach, Raman, and QTM relaxation pathways (Eqn. 1).

$$\tau^{-1} = \tau_0^{-1}\exp\left(-\frac{U_{eff}}{k_B T}\right) + CT^n + \tau_{QTM}^{-1} \qquad (1)$$

The best fit parameters to Eqn. 1 are C = 0.00185 $s^{-1}\cdot K^{-n}$, n = 3.38, τ_{QTM} = 0.0493 s, τ_0 = 2.75 x 10^{-8} and an effective relaxation barrier (U_{eff}) of 475 K / 330 cm^{-1}. The obtained barrier falls between the energies of the second (248 cm^{-1}, 243 cm^{-1}) and third (462 cm^{-1}, 457 cm^{-1}) KDs determined by *ab initio* calculations. Based on the analysis of the transition magnetic dipole moments (Table S11), calculations predict that the barrier should be crossed at earliest in the third KD, giving a barrier of *ca.* 460 cm^{-1}. The calculated value is in good agreement to the value obtained from the fit of the experimental data but is evidently overestimated (see the ESI for further information). This most likely results from neglect of electron correlation effects outside of the *4f* orbital space, which results in an underestimation of the contribution of $[BPh_4]^-$ and overestimation of the axiality of the complex. The

Raman exponent and τ_0 are similar to DyCp*$_2$BPh$_4$, and within the range of typical SMMs.[1,12] The rate of tunnelling in **1** of 4.92 ms is approximately three-times slower than DyCp*$_2$BPh$_4$ (1.42 ms), indicative of a slower through-barrier relaxation and reduced influence of QTM on the relaxation dynamics of **1**.

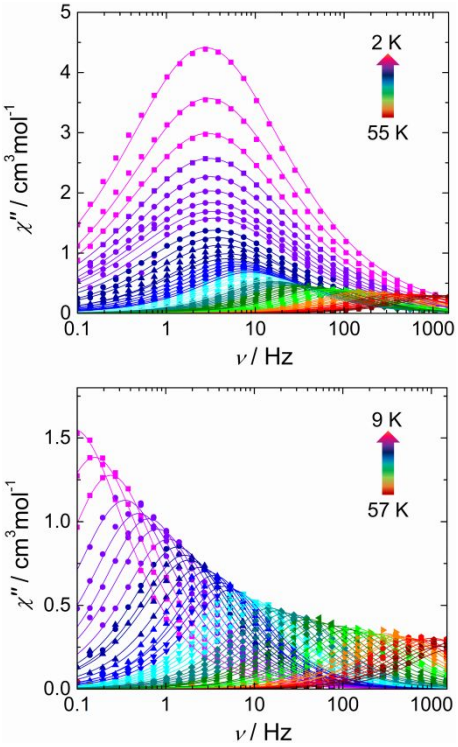

Fig. 2 Frequency dependence of the out-of-phase magnetic susceptibility (χ'') in the indicated temperature range for compound **1** in the absence of an applied static field (top) and in the presence of an applied field of 1000 Oe (bottom). Solid lines represent fits to the generalized Debye model which are summarized in Table S4 and S5.

As suggested by the S-shape character of the field dependence of the magnetization, magnetic blocking may be present in **1**. Therefore, hysteresis measurements were performed using a mean-field sweep rate of 14.01 Oe/s (-2 kOe ≤ H_{dc} ≤ 2 kOe; Fig. S8). Under these conditions, waist restricted hysteresis is observable up to 6.5 K (Fig. 4). Magnetic relaxation is a temporal process and is ultimately defined by the rate of any particular experiment; therefore it is surprising that improvements in the hysteretic behaviour is observable despite the comparatively slower sweep rate that is used for DyCp*$_2$BPh$_4$ (20 Oe/s) which displays similar butterfly-shaped behaviour up to only 5.8 K. This type of crossing at H_{dc} = 0 Oe is often attributed to efficient ground state QTM which is also confirmed by the AC magnetic susceptibility measurements. Despite improvements in the relaxation dynamics of **1,** contributions from QTM are still present at low temperatures, and thus neither complex shows open hysteresis when H_{dc} = 0 Oe.

Given the limited frequency dependence of τ at low-temperatures, investigation into the field dependence of the relaxation was undertaken. Applied dc fields ranging from 0-1800 Oe at 10 K elicits a noted sensitivity to the external magnetic field (Fig. S9), resulting in the appearance of a well-

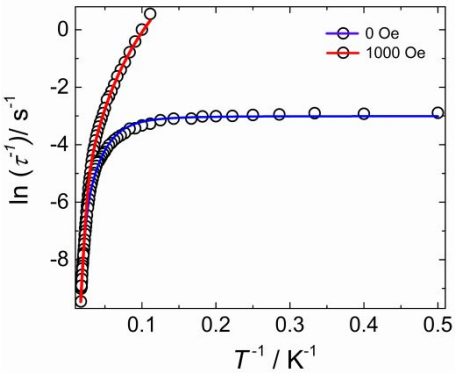

Fig. 3 Temperature dependence of the relaxation times (τ) in the absence (H_{dc} = 0 Oe; blue) and in the presence (red) of an applied static field of 1000 Oe in the range of 2-57 K. The solid line represents the sum of the Orbach, Raman and Quantum Tunnelling relaxation mechanisms (Eqn. 1; main text). Parameters are summarized in Table S6

defined peak shifted towards lower frequencies (<0.2 Hz at 1000 Oe). This is accompanied by the rapid disappearance of the original process with increasing field strengths. By extracting τ under an applied static field using the generalized Debye model, the field-dependent $\chi''(\nu)$ revealed a significant increase in τ upon application of an external magnetic field (Table S7) up to a strength of 1000 Oe (0.95 *vs*. 0.050 s). Above this, no appreciable increase in τ is observed, even up to fields strengths as high as 1800 Oe. This field (H_{dc} = 1000) also coincides with the point at which the inclusion of two Debye terms is no longer necessary to accurately reproduce the data, indicating that complete suppression of the secondary high-frequency peak is attainable at fields of 1000 Oe and above.

To provide a meaningful comparison of the contributions from the different relaxation mechanisms as well as enhance the slow-relaxation properties by inhibiting the deleterious field-dependent relaxation pathways, ac susceptibility was collected in the presence of an external field of 1000 Oe. Frequency-dependent behaviour is present over the full temperature range of 9-57 K, indicating the effects of QTM were effectively reduced with the application of an external magnetic field as a consequence of the m_j states being shifted out of resonance with one another. The plot of $ln(\tau)$ *vs.* T^{-1} obtained from the $\chi''(\nu)$ displays a linear region attributed to a thermally activated Orbach process up to 37 K (Fig. 3), at which point the Raman process takes over, with no temperature independence being realized for this data set. The best-fit parameters to Eqn. 1 for the Raman term are C = 0.00015 $s^{-1}\cdot K^{-n}$, n = 3.86. Interestingly, the increase in the Raman exponent with application of a field is near-identical to that observed in DyCp*$_2$BPh$_4$ (n = 3.85) at H_{dc} = 1600 Oe, indicating that the temperature-dependence of the Raman relaxation in both complexes remains relatively unchanged. Slight improvements in the fitted energy barrier are also obtained (490 K / 340 cm^{-1}) which is consistent with the reduction of ground-state QTM upon application of an external magnetic field. Given the similarities in the Raman component of both complexes, the rate at which the Raman relaxation overtakes the thermally activated Orbach process offers a better point of comparison than the fitted parameters.